

**IN-PROCESS ROUGHNESS MEASUREMENT  
AND TOOL NOSE RADIUS WEAR ASSESSMENT  
IN FINISH TURNING USING MACHINE VISION**

**MOHAN KUMAR BALASUNDARAM**

**UNIVERSITY SAINS MALAYSIA**

**2017**

**IN-PROCESS ROUGHNESS MEASUREMENT AND TOOL  
NOSE RADIUS WEAR ASSESSMENT IN FINISH TURNING  
USING MACHINE VISION**

**by**

**MOHAN KUMAR BALASUNDARAM**

**Thesis submitted in fulfillment of  
the requirements for the degree of  
Doctor of Philosophy**

**June 2017**

## **ACKNOWLEDGMENTS**

First of all, I would like to express my heartfelt gratitude to my supervisor, Professor Dr. Mani Maran Ratnam, for his support and motivation throughout this research work. His guidance and incisive advice have inspired me to generate fruitful approaches in achieving the objectives of this research. Without his effort, I would not be able to proceed and bring this research to a completion.

My special thanks go to all the academic staffs of School of Mechanical Engineering, University Sains Malaysia, who in one way or another gave their valuable advice throughout this journey.

My heartfelt gratitude is extended to my late mother, beloved father, brother and sisters that support me unlimitedly all along without any hesitation. I dedicate my special appreciation to my wife and kids that gives me strength along the six years of study journey. I treasure dearly their encouragement and moral support throughout these years.

## TABLE OF CONTENTS

	<b>Page</b>
<b>ACKNOWLEDGEMENTS</b>	ii
<b>TABLE OF CONTENTS</b>	iii
<b>LIST OF TABLES</b>	viii
<b>LIST OF FIGURES</b>	x
<b>LIST OF SYMBOLS</b>	xvii
<b>LIST OF ABBREVIATIONS</b>	xix
<b>ABSTRAK</b>	xxi
<b>ABSTRACT</b>	xxii
<b>CHAPTER ONE : INTRODUCTION</b>	
1.1 In-process roughness measurement	1
1.2 Problem Statement	3
1.3 Research objectives	5
1.4 Research Scopes	6
1.5 Thesis Outline	9
<b>CHAPTER TWO : LITERATURE REVIEW</b>	
2.1 Introduction	8
2.2 Surface roughness measurement in turning	8
2.2.1 Surface roughness measurement in turning process using machine vision approach	9
2.2.2 Surface roughness measurement in other machining processes using machine vision approach	12
2.2.3 Sensor approach for in-process surface roughness assessment	16
2.3 Tool wear monitoring (TWM) in turning	20
2.3.1 Direct TWM using machine vision	23
2.3.2 Indirect TWM using machine vision	28

2.3.3	Indirect TWM using sensors	32
2.3.4	Indirect TWM using multi-sensor approach	41
2.4	Sub-pixel edge location	46
2.5	Research gaps identified in the literature	47
2.6	Summary	48

### **CHAPTER THREE : METHODOLOGY**

3.1	Introduction	49
3.2	Measurement of surface roughness of a rotating workpiece	51
3.2.1	Workpiece preparation	51
3.2.2	Machine vision system configuration	51
3.2.3	Determination of scaling factor and assessment of image distortion	55
3.2.4	Image acquisition and surface roughness measurement of a rotating pre-turned workpiece	59
3.2.5	Edge detection algorithm and extraction of surface roughness profile for the roughness measurement	60
3.2.6	Sub-pixel edge detection using invariant moment method and roughness measurement	62
3.3	Study on the effect of rotational speed on the surface roughness measurement accuracy	66
3.4	In-process roughness measurement in dry and wet finish turning process	67
3.4.1	System configuration used for dry finish turning process	67
3.4.2	System configuration used for wet finish turning process	70
3.5	Study on the effect of machining time on surface roughness in dry turning	71
3.5.1	System setup	73
3.5.2	Assessment of image distortion	74
3.5.3	Determination of the amplitude, hybrid, spacing and functional surface roughness parameters	75

3.5.4	Surface roughness analysis of turned surface with new roughness parameters	82
3.6	Image acquisition using CCD camera	84
3.7	Assessment of nose radius wear from workpiece roughness profile	89
3.8	In-process nose radius wear assessment in wet finish turning process	94
3.9	Summary	97

#### **CHAPTER FOUR : RESULTS AND DISCUSSIONS**

4.1	Introduction	99
4.2	Image distortions assessment	99
4.2.1	Distortion assessment in the $x$ and $y$ - direction	99
4.3	Study on the effect of workpiece rotational speed on the surface roughness measurement accuracy	103
4.4	In-process roughness measurement in dry and wet finish turning process	117
4.5	Effect of machining duration on surface roughness in dry finish turning process	122
4.5.1	Verification of in-process surface roughness measurement for hybrid spacing and functional surface roughness parameters	128
4.5.2	Effect of machining duration on surface roughness	131
4.5.3	Effect of machining duration on amplitude parameters	131
4.5.4	Effect of machining duration on spacing and hybrid parameters	136
4.5.5	Effect of machining duration on bearing area curve parameters	142
4.5.6	Effect of machining time on new roughness parameters	146
4.6	Assessment of tool nose radius wear from roughness parameters during wet finish turning	150

4.6.1	Verification of in-process surface roughness measurement for hybrid spacing and functional surface roughness parameters in wet finish turning.	150
4.6.2	Correlation between the tool nose radius wear and amplitude roughness parameters	158
4.6.3	Correlation between tool nose radius wear with spacing and hybrid roughness parameters	163
4.6.4	Correlation between bearing area curve parameters and tool nose wear	167
4.6.5	Correlation between new roughness parameters and tool wear	170
4.7	Summary	179

## **CHAPTER FIVE : CONCLUSIONS**

5.1	Conclusions and contributions of research	185
5.2	Recommendations and Future study	188

<b>REFERENCES</b>	189
-------------------	-----

## **APPENDICES**

Appendix A	Surface roughness obtained using stylus method for specimen 1 to 5 and 7.
Appendix B	Images of workpiece and surface roughness profile for specimen 1 to 5 and 7.
Appendix C	Surface roughness obtained using stylus method in dry turning (cutting speed: 100 m/min and feed: 0.1 and 0.2 mm/rev)
Appendix D	Surface roughness obtained using vision method in dry turning (cutting speed: 100 m/min and feed: 0.1 and 0.2 mm/rev)

- Appendix E Surface roughness parameters as a function of machining time in dry turning (feed:0.1 and 0.2 mm/rev)
- Appendix F Surface roughness obtained using stylus method in wet turning (cutting speed 149.15 m/min and feed: 0.15 and 0.25 mm/rev)
- Appendix G Surface roughness obtained using vision method in wet turning (cutting speed 149.15 m/min and feed: 0.15 and 0.25 mm/rev)
- Appendix H Cutting conditions adopted in different stages of experimentation.

## **LIST OF PUBLICATIONS**



## LIST OF TABLES

		Page
Table 3.1	Specifications of surface roughness parameters.	76
Table 4.1	Centroid distance error for $x$ -directional calibration of small dots.	101
Table 4.2	Centroid distance error for $y$ -directional calibration of small dots.	102
Table 4.3	Roughness parameters determined using stylus method	103
Table 4.4	Average roughness ( $R_a$ ) determined using vision method.	107
Table 4.5	Root mean square roughness ( $R_q$ ) determined using vision method.	108
Table 4.6	Peak-to-valley height ( $R_t$ ) determined using vision method.	109
Table 4.7	Comparison between roughness values ( $R_a$ , $R_q$ and $R_t$ ) determined for 4000 rpm using machine vision method and stylus method.	110
Table 4.8	Performance indices for roughness measurements at different spindle speed.	113
Table 4.9	Comparison between roughness values ( $R_a$ ) determined using machine vision method at different spindle speed and stylus method.	114
Table 4.10	Comparison between roughness values ( $R_q$ ) determined using machine vision method at different spindle speed and stylus method.	115
Table 4.11	Comparison between roughness values ( $R_t$ ) determined using machine vision method at different spindle speed and stylus method.	116

Table 4.12	Comparison between roughness determined using vision method and stylus method in dry and wet turning.	121
Table 4.13	Roughness obtained in the same zone of the workpiece using vision method in different interval of machining time in dry turning.	126
Table 4.14	Comparison between hybrid parameters obtained using vision method and stylus method.	129
Table 4.15	Comparison between bearing area curve parameters obtained using vision method and stylus method.	130
Table 4.16	Roughness obtained using vision method in different intervals of machining time.	154
Table 4.17	Comparison between hybrid parameters obtained using vision method and stylus method.	156
Table 4.18	Comparison between bearing area curve parameters obtained using vision method and stylus method	157
Table 4.19	Coefficient of determination ( $R^2$ ) between roughness parameters and nose radius wear for 0.4mm/rev feed.	175
Table 4.20	Coefficient of determination ( $R^2$ ) between roughness parameters and nose radius wear at different cutting conditions.	180

## LIST OF FIGURES

		<b>Page</b>
Figure 2.1	Typical cutting tool wear.	20
Figure 2.2	(a) Top view of crater wear and nose profile. (b) flank wear land and notch wear of cutting tool based on ISO 3685 (1993).	21
Figure 3.1	Flow chart of overall methodology of vision based in-process surface roughness measurement tool nose radius wear assessment.	50
Figure 3.2	Schematic diagram of the experimental setup.	52
Figure 3.3	Actual setup of roughness measurement system.	53
Figure 3.4	Actual set-up showing the image capture direction.	54
Figure 3.5	(a) System setup to capture the image of the pin gage (b) Pin gage image to find the horizontal scaling factor and (c) Pin gage image to find the vertical scaling factor.	56
Figure 3.6	Distortion grid target (MIL-STD-45662A).	57
Figure 3.7	System set up to capture the image of grid target.	57
Figure 3.8	(a) Small grid pattern used for $x$ - and $y$ -directional distortion assessment (b) Grid dimension and (c) centroid distance (CD).	58
Figure 3.9	Small grid pattern captured for distortion assessment.	58
Figure 3.10	Edge image of the surface profile of the rotating specimen (4000 rpm).	60
Figure 3.11	Flow chart showing the various stages of image processing algorithm.	61
Figure 3.12	Sample of an ideal edge step edge for gray profiles.	62

Figure 3.13	Workpiece surface profile and sub-pixel edge location.	64
Figure 3.14	Orthogonal scanning of surface profile with sub-pixel edge location.	65
Figure 3.15	Backlighting arrangement for in-process roughness measurement.	69
Figure 3.16	Image of the cutting insert and workpiece surface profile and the direction of chips disposed during turning.	69
Figure 3.17	Successive images of surface profile captured during dry turning.	70
Figure 3.18	Edge image of surface roughness profile.	71
Figure 3.19	(a) System configuration used in wet finish turning process (b) image of the cutting insert and workpiece surface profile and the direction of chips disposed.	72
Figure 3.20	Schematic illustration of the experimental setup.	73
Figure 3.21	Actual setup of in-process surface roughness measurement in continuous dry turning.	74
Figure 3.22	Images of Ronchi rulings (a) – (b) 50 mm	75
Figure 3.23	(a) Surface roughness profile (b) Amplitude density function (ADF)	77
Figure 3.24	Surface roughness profile and description of the intercepted length to determine the bearing area length (ISO 13565 norms).	78
Figure 3.25	The bearing area curve of the surface roughness profile.	79
Figure 3.26	The bearing area curve fitted with a straight line corresponding to 40%.	80
Figure 3.27	The bearing area curve and the respective parameters.	81

Figure 3.28	Tool-workpiece interface capture using CCD camera.	82
Figure 3.29	Calculation of (a) the profile slope (b) relative length.	84
Figure 3.30	System set up used to capture the image of tool nose region.	85
Figure 3.31	System set up used to capture the image of tool nose tool nose region (with ND filter).	86
Figure 3.32	System set up used to capture the image of tool-workpiece interface.	86
Figure 3.33	Tool nose profile captured by the CCD camera with ND filter.	87
Figure 3.34	CCD Image of tool-workpiece interface.	88
Figure 3.35	Alicona InfiniteFocus, 3-D metrology system.	88
Figure 3.36	Schematic of the tool-workpiece interface.	89
Figure 3.37	Schematic of the nose region of tool before and after tool wear.	90
Figure 3.38	Schematic of the workpiece surface profile formed by new and worn cutting tool.	91
Figure 3.39	Schematic of turning operation using a cutting tool.	92
Figure 3.40	Section <i>A-A</i> of Figure 3.39.	92
Figure 3.41	Enlarged region of interest in Figure 3.40.	93
Figure 3.42	Actual setup of in-process tool nose radius wear assessment system.	95
Figure 3.43	Flow chart for the in-process tool nose radius wear assessment.	96
Figure 4.1	Average centroid distance errors for <i>x</i> directional calibration of small dots.	101
Figure 4.2	Average centroid distance errors for <i>y</i> directional calibration of small dots.	102

Figure 4.3	Images of work piece and roughness profiles at different spindle speeds (Specimen 6).	104
Figure 4.4	Correlation of roughness ( $R_a$ ) between vision and stylus method (4000 rpm).	112
Figure 4.5	Correlation of roughness ( $R_q$ ) between vision and stylus method (4000 rpm).	112
Figure 4.6	Correlation of roughness ( $R_t$ ) between vision and stylus method (4000 rpm).	113
Figure 4.7	Edge images of work piece and surface profile at a cutting speed of 58.85 m/min.	118
Figure 4.8	Edge images of work piece and surface profile at a cutting speed of 89.50 m/min.	119
Figure 4.9	Edge images of work piece and surface profile at a cutting speed of 108.33 m/min.	120
Figure 4.10	Image of cutting tool and workpiece captured using CCD camera.	123
Figure 4.11	Images of workpiece and roughness profiles at different machining times in dry turning	124
Figure 4.12	$R_a$ as a function of machining time.	132
Figure 4.13	Comparison between workpiece surface profiles (a) new tool, (b) after 120 minutes of machining time	132
Figure 4.14	$R_t$ as a function of machining time.	133
Figure 4.15	Surface roughness profile of typical turning process.	134
Figure 4.16	$R_{sk}$ as a function of machining time.	135
Figure 4.17	$R_{kt}$ as a function of machining time.	136
Figure 4.18	$R_{sm}$ as a function of machining time.	137
Figure 4.19	$P_c$ as a function of machining time.	138
Figure 4.20	$RA_q$ as a function of machining time.	138

Figure 4.21	Surface profile of machined surface produced by (a) new tool, (b) after 120 min of machining time.	140
Figure 4.22	$R\lambda_a$ as a function of machining time.	141
Figure 4.23	$R_{pk}$ as a function of machining time	143
Figure 4.24	$R_k$ as a function of machining time.	144
Figure 4.25	$R_{vk}$ as a function of machining time.	144
Figure 4.26	$Mr_1$ as a function of machining time.	145
Figure 4.27	$Mr_2$ as a function of machining time.	146
Figure 4.28	$\Phi_p$ as a function of machining time	147
Figure 4.29	Measurement of average slope of profile peaks ( $\Phi_p$ ) and average slope of profile valleys ( $\Phi_v$ )	148
Figure 4.30	$\Phi_v$ as a function of machining time.	148
Figure 4.31	Measurement of the relative length of profile ( $R_{rl}$ ).	149
Figure 4.32	$R_{rl}$ as a function of machining time.	149
Figure 4.33	Images of workpiece and roughness profiles at different machining times in wet turning.	151
Figure 4.34	Sample image of cutting tool captured using CCD camera at various machining time in wet finish turning and the corresponding nose wear areas.	159
Figure 4.35	Correlation between tool nose radius wear and $R_a$ .	160
Figure 4.36	Correlation between tool nose radius wear and $R_r$ .	161
Figure 4.37	Correlation between tool nose radius wear and Skewness ( $R_{sk}$ ).	162
Figure 4.38	Correlation between tool nose radius wear with Kurtosis ( $R_{kt}$ ).	162
Figure 4.39	Correlation between tool nose radius wear and $R\Delta_q$ .	163
Figure 4.40	Correlation between tool nose radius wear and $R\Delta_a$ .	164

Figure 4.41	Correlation between tool nose radius wear and $R\lambda_a$ .	165
Figure 4.42	Correlation between tool nose radius wear and $R\lambda_q$ .	165
Figure 4.43	3-D surface profile produced by worn tool of machined at 149.15 m/min.	166
Figure 4.44	Correlation between tool nose radius wear with $R_{pk}$ .	167
Figure 4.45	Correlation between tool nose radius wear with $R_{vk}$ .	168
Figure 4.46	Correlation between tool nose radius wear with core roughness depth ( $R_k$ )	169
Figure 4.47	Correlation between tool nose radius wear with $Mr1$ .	169
Figure 4.48	Correlation between tool nose radius wear with $Mr2$ .	170
Figure 4.49	Correlation between tool nose radius wear with $\Phi_p$ .	171
Figure 4.50	Correlation between tool nose radius wear with $\Phi_v$ .	171
Figure 4.51	Correlation between tool wear with $R_{rl}$ .	172
Figure 4.52	SEM images of new cutting tool.	172
Figure 4.53	SEM images of worn-out insert captured after 280 min of machining time	173
Figure 4.54	SEM images (a) continuous chip generated by new tool and (b) serrated chip generated by worn tool after 280 min of machining time.	174
Figure 4.55	Amplitude roughness parameters and the correlation coefficient.	176
Figure 4.56	Hybrid roughness parameters and the correlation coefficient.	176
Figure 4.57	Bearing area curve parameters and the correlation coefficient.	177
Figure 4.58	New parameters and the correlation coefficient.	177



Figure 4.59	Sample image of cutting tool captured using CCD camera at various machining time and the corresponding nose wear areas. (feed = 0.25 mm, cutting speed = 149.15 m/min).	178
Figure 4.60	Amplitude roughness parameters and the correlation coefficient.	181
Figure 4.61	Hybrid roughness parameters and the correlation coefficient.	181
Figure 4.62	Bearing area curve parameters and the correlation coefficient.	182
Figure 4.63	New parameters and the correlation coefficient.	182

## LIST OF SYMBOLS

<b>Symbol</b>	<b>Description</b>
$A1$	Quantity of solid peaks
$A2$	Quantity of solid valleys
$f$	Feed rate
$F_z, F_x$	Cutting force tangential and feed direction
$G_a$	Arithmetic average of gray level
$h$	Background intensity
$k$	Edge contrast
$M_{r1}$	Material ratio 1 at the peak zone of the profile
$M_{r2}$	Material ratio 2 at the valley zone of the profile
$p_1, p_2$	Pixel densities
$P_c$	Peak count of the roughness profile
$p_h$	Number of samples with gray level $h$
$R_a$	Arithmetic average height roughness parameter
$r_e$	Tool nose radius
$R_k$	Core roughness depth of the roughness profile
$R_{ku}$	Kurtosis of the roughness profile height distribution
$R_{pk}$	Reduced peak height of the roughness profile
$R_q$	Root mean square roughness parameter
$R_{rl}$	Relative length ratio of the peaks
$R_{sk}$	Skewness of the roughness profile height distribution
$R_{Sm}$	Mean line peak spacing of the roughness profile

$R_t$	Maximum peak to valley height roughness parameter
$R_{vk}$	Reduced valley depth of the roughness profile
$R_z$	Ten point average height roughness parameter
$RA_a$	Average profile slope
$RA_q$	Root mean square profile slope
$RA_\lambda$	Average wavelength of the roughness profile
$RA_\lambda$	Root mean square average wave length of the profile
$s$	Skewness of the input image data sequence
$SD$	Standard deviation
$U_{Ex}$	Uncertainty
$VB$	Average width of the flank wear land
$V_{BA}, V_{BB}$	Flank wear land
$VB_{max}$	Maximum width of the flank wear land
$V_x, V_y$ and $V_z$	Amplitude of vibration components in x y and z directions
$\Phi_p$	Average slope of the profile peaks of the profile
$\Phi_v$	Average slope of the profile valleys of the profile
$m_1, m_2, m_3$	First three moments in the gray scale image
$\theta_m$	Mean slope of the roughness profile

## LIST OF ABBREVIATIONS

ADF	Amplitude Density Function
AE	Acoustic Emission
AHD	Asperities' height distribution
AI	Artificial Intelligence
AISI	American Iron and Steel Institute
ANFIS	Artificial Neuro-Fuzzy Interference System
ANN	Artificial Neural Network
AOE	Acousto-optic Emission
ARMA	Autoregressive moving average
BAC	Bearing Area Curve
B-K	Beckmann–Kirchhoff
CCD	Charge-coupled Device
CD	Centroidal Distance
DOV	Degree of Overlap
DSLR	Digital Single-Lens Reflex
DWT	Discrete wavelet transforms
FFBP	Feed Forward Back Propagation
FFT	Fast Fourier Transform
FOV	Field of View
GLCM	Grey-level Co-occurrence Matrix
I-MR	Individual and Moving Range
ISO	International Standard Organization

LS-SVM	Least-Squares Support Vector Machines
MLP-ANN	Multilevel Perception Artificial Neural Network
ND	Neutral Density
RMS	Root Mean Square
ROI	Region of Interest
SEM	Scanning Electron Microscopy
SF	Scaling Factor
TCM	Tool Condition Monitoring
TWM	Tool Wear Monitoring

**PENGUKURAN KEKASARAN DAN PENILAIAN PENGHAUSAN JEJARI  
MUNCUNG MATA ALAT DALAM PROSES LARIKAN PENYUDAHAN  
MENGUNAKAN PENGLIHATAN MESIN**

**ABSTRAK**

Pengukur kekasaran berasaskan jarum yang biasanya digunakan untuk mengukur kekasaran permukaan pada komponen yang dilarik tidak sesuai untuk pengukuran kekasaran semasa pemesinan. Dalam kajian ini, kaedah baharu untuk menilai kekasaran permukaan bahan kerja dan kehausan jejari muncung mata alat semasa proses melarik menggunakan mesin penglihatan dicadangkan. Kamera digital kanta balikan tunggal dengan kelajuan pengatup tinggi diletak bertentangan pada mata alat telah digunakan untuk mengambil gambar bayangan bebas kabur pada bahan kerja. Profil kekasaran telah disari pada tahap kejituan sub-piksel daripada gambar yang diambil menggunakan algoritma daripada MATLAB. Daripada profil yang disari, amplitud, penjarakan, hibrid dan juga parameter kekasaran permukaan kefungsiian telah ditentukan. Tiga parameter kekasaran permukaan baharu iaitu purata kecerunan profil puncak ( $\Phi_p$ ), purata kecerunan profil lurah ( $\Phi_v$ ), panjang puncak relatif ( $R_{rl}$ ), telah diperkenalkan untuk mengkaji sisihan mikrojeometri dalam profil kekasaran permukaan oleh kerana kehausan jejari muncung mata alat. Perbandingan antara pengukuran kekasaran permukaan ketika pemesinan dan juga bacaan kekasaran permukaan yang diperoleh menggunakan jarum pengukur kekasaran mudah alih menunjukkan kaedah yang diusulkan dapat memberi bacaan kekasaran permukaan dengan sisihan maksimum 9.2%. Antara parameter kekasaran permukaan yang dianalisis, purata panjang gelombang ( $R\lambda_a$ ) bagi profil kekasaran permukaan dan min kecerunan ( $R\lambda_a$ ) untuk profil menunjukkan korelasi terbaik dengan kehausan jejari muncung mata alat dengan nilai  $R^2$  antara 0.9881 dan 0.9757 masing-masing. Kaedah berasaskan penglihatan tak sentuh yang dibangunkan dalam kajian ini membolehkan penilaian yang tepat bagi kekasaran permukaan bahan kerja dan kehausan jejari muncung mata alat dalam pelarikan kemas.

## IN-PROCESS ROUGHNESS MEASUREMENT AND TOOL NOSE RADIUS WEAR ASSESSMENT IN FINISH TURNING USING MACHINE VISION

### ABSTRACT

The stylus roughness tester used for measuring the surface roughness of a turned part is unsuitable for in-process roughness measurement. In this research, a novel approach for the assessment of the surface roughness of the workpiece and the tool nose radius wear during the turning process using machine vision is proposed. A digital single-lens reflex camera with a high shutter speed was used to capture a blur-free silhouette image of the rotating workpiece profile diametrically opposite the cutting tool. The roughness profile was extracted with sub-pixel level accuracy from the captured image using algorithms developed in MATLAB. From the extracted profile, the amplitude, spacing, hybrid as well as the functional surface roughness parameters were determined. Three new roughness parameters, namely the average slope of profile peaks ( $\Phi_p$ ), average slope of profile valleys ( $\Phi_v$ ), relative length of peaks ( $R_r$ ), were introduced to study the micro geometrical deviation in the surface roughness profile due to the tool nose radius wear. Comparison of the in-process roughness measurement and the surface roughness values obtained using a portable stylus roughness tester showed that the proposed method is able to measure the roughness parameters with a maximum deviation of 9.2%. Among the existing surface roughness parameters analysed the average wavelength ( $RL_a$ ) of roughness profile and the mean slope ( $RA_a$ ) of the profile showed the best correlation with the tool nose radius wear with coefficient of determination ( $R$ -squared) values of 0.9881 and 0.9757, respectively. The non-contacting vision based method developed in this research enables accurate assessment of the surface roughness of the workpiece and tool nose radius wear in finish turning.

## CHAPTER ONE

### INTRODUCTION

#### 1.1 In-process roughness measurement

Turning is an important industrial machining process used to remove material from a workpiece using a single point cutting tool. Rough turning is used to remove the material from the workpiece to achieve the required dimension while finish turning is used to achieve high dimensional accuracy and good surface finish quality. The surface finish quality of a machined part is affected by factors such as the machining conditions, material hardness, cutting edge geometry and tool wear. Tool wear is categorized into flank wear, crater wear, notch wear, nose radius wear, edge chipping, edge cracking, plastic deformation and gross fracture (Bhuiyan and Choudhury, 2015). Among these, flank wear remains the most commonly used measure of tool wear. However, in finish turning process the tool nose radius wear dominates and directly influences the quality of the surface finish since the cutting action is undertaken by the tool nose edge.

Surface roughness measurement is carried out to ensure that the surface finish quality of a machined part conforms to its specification. In general, the surface roughness measurement methods can be divided into two types, namely contact and non-contact methods. Mechanical stylus is a well-established and standard contact method for the roughness measurement of turned parts. In this method, a stylus is drawn across the machined surface and the minute fluctuations of the stylus in the vertical directions are amplified and recorded. The roughness parameters are then computed from the vertical fluctuations of the stylus. Although the mechanical stylus method provides reliable surface roughness measurement, getting access to



the workpiece surface for roughness measurement during the turning process is not possible due to the high surface speed of the rotating workpiece. Thus, the stylus method is not suitable for in-process surface roughness measurement. However, in-process surface roughness measurement in finish turning process is important in manufacturing since real time measurement of the surface roughness decreases machine down time and increases productivity. Moreover, since the cutting tool leaves an imprint on the workpiece surface finish the in-process surface roughness measurement provides a real time indication on the condition of the cutting tool, thus ensuring timely replacement of a worn out tool.

Non-contact roughness measurement using optical and non-optical methods have advantages over the stylus methods, such as the ability for in-process, rapid measurement capability, no parts that wear due to the non-contact nature, and the ability to provide information over a surface area (Shahabi and Ratnam, 2009b). The non-contact techniques proposed in the past for in-process surface roughness measurement can be generally divided into optical and non-optical methods (Guo and Tao, 2013). The light scattering and speckle contrast methods are the most widely studied optical methods (e.g. Suksawat, 2011; Kirby et al. 2006). The commonly used non-optical methods are cutting force, vibration, cutting temperature and ultrasonic methods (e.g. Somkiat and Voraman, 2012; Suhail et al. 2011; Salgado et al. 2009). Although several authors have implemented the non-contact methods for in-process surface roughness measurement, these methods are capable of providing only the basic amplitude surface roughness parameters, such as average roughness ( $R_a$ ) and root-mean-square roughness ( $R_q$ ). These basic amplitude parameters give only an indication of the roughness amplitude and are insensitive to the spatial wavelength of the workpiece profiles.

Moreover, none of the non-contact methods developed in the past is capable of measuring the numerous amplitude, spacing, hybrid parameters as well as functional parameters. To date, the measurement of all these parameters can only be done by using the stylus instrument.

Machine vision method of surface roughness measurement coupled with image processing has received a great deal of attention in the past (Guo and Tao, 2013; Dhanasekar and Ramamoorthy, 2010). However, to date, only the measurement of the basic amplitude surface roughness parameters from the turned workpiece surface using machine vision methods have been reported. Most of these methods are limited to stationary surfaces.

## **1.2 Problem Statement**

In most of the published literature involving study on surface roughness measurement in turning, the authors either removed the workpiece from the lathe for roughness measurement or measured the roughness in-situ, i.e. without removing the workpiece. In either case it is necessary to stop the machine thus interrupting the turning process. The most commonly used contact stylus methods for surface roughness measurement are not suitable for in-process surface roughness measurement, especially when the workpiece is spinning at high speeds during the turning process. To overcome the limitations of the stylus methods for in-process surface roughness measurement, non-contact methods have been developed.

Among the non-contact methods, the optical techniques based on light scattering and speckle contrast have been reported in the literature for in-process surface roughness measurement. However, the in-process optical

techniques developed in the past are capable of measuring only the basic amplitude surface roughness parameters.

The sensor based non-optical techniques for in-process surface roughness measurement are not capable of measuring the numerous amplitude, spacing, hybrid parameters as well as the functional parameters, since most sensors are capable of detecting only the root-mean-square (RMS) value of the signal. However, to investigate the correlation between the surface roughness parameters and the cutting tool conditions, roughness parameters other than the basic parameters need to be measured during turning. Ideally, the in-process roughness measurement system should combine the potential of the stylus method in measuring the numerous surface roughness parameters and the rapidness of the non-contacts methods in measuring the roughness parameters from the workpiece surface. Moreover, an in-process study on the micro geometric variations in the workpiece surface profile caused by the progressive tool nose radius wear has not been reported.

Despite the benefits of the sensor based tool condition monitoring using acoustic emission, cutting force, vibration and ultrasonic, the use of sensors for in-process tool condition monitoring adds complexity to the overall machining arrangement. Moreover, the main limitations of sensor based tool condition monitoring lie in the difficulty of placing the sensor in close vicinity of the cutting action, making them exposed to the heat, chips and coolant, thus affecting the performance of the sensors and also the quality of measurements. In addition, the signal from the sensor contains information other than the tool condition which comes from the machine tool vibration, chip removal, and environmental noise. Hence, the signals collected by the sensors require further processing to assess the

tool condition. Although the sensor fusion using the neural network-based system has been developed for tool condition monitoring, the extensive training of the neural networks is still a drawback.

The simplicity of capturing and analyzing images of the machined surfaces using machining vision system with a CCD camera has encouraged researchers in the past to use the roughness parameters for tool condition monitoring. However, the image acquisition using a CCD camera has the disadvantage of providing a small field-of-view at high optical magnification, low resolution and non-uniform illumination depending on the lighting and blurring effect due to rotation of the workpiece. Moreover, the recent developments in roughness measurement using machine vision is only limited to pixel level accuracy. For precise measurement of surface roughness of rotating workpiece during turning process, the edge of the workpiece profile must be determined to sub-pixel accuracy. Even though it is often quoted in the literature on tool condition monitoring that the monitoring of the tool wear during machining improves the quality of machined parts, reduce production time and save costs, to date, no published works have been reported on the tool nose radius wear monitoring based on the workpiece surface roughness parameter during dry and wet finish turning process.

### **1.3 Research objectives**

The objectives of the research are as follows:

- To develop a non-contact machine vision method for measuring the surface roughness of a rotating workpiece during dry and wet finish turning.
- To study the effect of machining time on the workpiece surface roughness parameters in finish turning.

- To introduce new surface roughness parameters to study the effect of micro geometric variations in the surface profile caused by tool nose radius wear.
- To evaluate the tool nose radius wear monitoring effectiveness based on the workpiece surface roughness parameter in finish turning.

#### **1.4 Research Scopes**

This research is focused on the development of a non-contact vision method for the in-process surface roughness measurement of a rotating work piece in dry and wet finish turning. The research comprises the calibration of the machine vision system, selection of an ideal shutter speed of the camera and the suitable lighting conditions.

This research also focuses on the accuracy study of roughness measurement, in-cycle tool nose radius wear measurement, study on the nose radius wear effect on the surface roughness, and tool wear monitoring from the workpiece surface profile in wet and dry finish turning operation. The scope of this research also includes the extraction of the amplitude, hybrid, and spacing, functional roughness parameters from the 2D silhouette edge image of the turned workpiece surface using a localized sub-pixel edge detection algorithm to locate the exact edge of workpiece roughness profile. The roughness measurement results obtained from the machine vision system were compared with the measurement from the portable stylus roughness tester to determine the accuracy of the measurement. The precision of measurement using machine vision system was investigated by varying the spindle speed of the lathe machine. This research also focuses on the effectiveness study of the in-process measurement system in wet and dry finish turning process to assess the tool nose radius wear from workpiece surface profile.

## **1.5 Thesis Outline**

This thesis is arranged in accordance to the scopes and objectives as mentioned above. Chapter 2 reviews the work related to the in-process surface roughness measurement and tool condition assessment and provides an overview from the published literature. A thorough discussion will be made to identify the advantages and limitations of the existing in-process approaches in assessing the surface roughness and tool condition assessment in turning process. Chapter 3 presents the methodology of the research in accordance to the scopes and objectives. The experimental setup and the development of image processing algorithms for surface roughness measurement as well as the accuracy for comparison of measurement approaches are detailed in this chapter. This is followed by the results and discussions in Chapter 4 which corresponds to each stage of experiments conducted. Subsequently, conclusions of this research are drawn in Chapter 5. Recommendations and suggestions are given for future work.

## **CHAPTER TWO**

### **LITERATURE REVIEW**

#### **2.1 Introduction**

In this chapter, a review of online surface roughness measurement and tool wear monitoring in a turning process using machine vision will be made based on the published literature. Sensor approach used for the in-process surface roughness estimation and tool condition monitoring are briefly reviewed. The term “in-process” or “on-line” refers to the measurement during machining while the terms “in-cycle” or “in-situ” refers to the measurement between machining cycles.

#### **2.2 Surface roughness measurement in turning**

The surface roughness measurement method is generally categorized as contact and non-contact. In the contact method, the surface roughness of a turned part is measured directly with a stylus roughness tester after the turning process. A stylus is drawn along the workpiece surface and the vertical movement of the stylus is used to calculate the surface roughness parameters. The stylus method, however, is not suitable for measuring the surface roughness of a rotating workpiece being machined during turning process.

Non-contacting methods have been developed using the optical and non-optical techniques to overcome the limitations of the contact method. A non-contact in-process surface roughness measurement method is desirable in the finish turning process to measure the entire workpiece surface quality without interruption of the machining process. The rapid in-process roughness measurement reduces the idle time of the machine tool, thus increasing the

productivity. In addition, an in-process surface roughness measurement can provide useful indications on the state of the cutting tool and ensure timely replacement of the worn out tool. The machine vision approach used for surface roughness measurement is discussed in the next section.

### **2.2.1 Surface roughness measurement in turning process using machine vision approach**

Several investigations have been carried out on measuring the surface roughness by using machine vision approach. Gupta and Raman (2001) developed a vision method to measure the surface roughness of a pre-turned rotating workpiece using images of the scattered spectrum of the laser light captured using a CCD camera. The surface roughness was characterized by the frequency distribution of the grey level occurrence in the scattered light intensity image. First order statistical texture descriptors were extracted based on the grey level histogram and used for interpreting the details of the images. The surface roughness was evaluated by the ratio of the RMS value of the histogram and its standard deviation. The results showed that the roughness was mostly affected by the cutting speed, whereas the other factors did not have any effect on the workpiece surface roughness.

Experiments were also conducted with and without lighting for different rotational speeds of the workpiece. It was found that ambient lighting did not affect the optical surface roughness parameter. Moreover, the rotation of the spindle did not have any effect on the roughness parameter. The authors commented that this technique can be employed for in-process application. However, the measurement was carried out on pre-turned workpiece and not during turning



process. The effects of coolant, reflectivity of the surface, chips and vibration on surface roughness measurement were not studied. Moreover, this method is limited to surfaces with uniform roughness distribution under the conditions of non-coherent light illumination.

Lee and Tarng (2001) proposed a vision system to capture the surface image of turned components machined with different combinations of cutting speed, feed and depth of cut. A digital single lens reflex camera with front-lighting was used to capture the surface image. The polynomial networks were used to predict the surface roughness based on the cutting parameters and arithmetic average of gray level ( $G_a$ ) parameter from the captured images. Cutting speed, feed, depth of cut and the image parameter  $G_a$  were given as input to the polynomial network. The results showed that this method was capable of measuring  $R_a$  with a maximum error of 4.6% compared to the stylus method. However, the roughness measurement experiments were performed on static condition of the turned work piece surface.

Lee et al. (2002) developed a vision system for measuring the surface roughness of turned parts. The images of the specimens acquired by the vision system were processed to obtain grey level parameters. The surface texture analysis was carried out on the images using the second order histogram or co-occurrence matrix of the images. The arithmetic average of gray level ( $G_a$ ) parameter was computed. The images were analyzed with and without chatter conditions. The variance, mean, and optical roughness parameter of the intensity distributions were calculated from the intensity histograms. However, in-cycle roughness measurement was carried out to measure the

parameter  $G_a$ . Lee et al. (2004) acquired surface image of turned steel work piece using DSLR camera with a diffused light source. An artificial neuro-fuzzy interference system (ANFIS) was used for the surface roughness estimation. The spatial frequency, arithmetic mean and standard deviation of grey level in the image were determined. The surface roughness was measured with an absolute deviation of  $\pm 8.7\%$  using the machine vision system. However, the roughness measurement was not conducted during the turning process.

Sarma et al. (2008) measured the  $R_a$  at different cutting conditions using the images of turned surfaces. The  $G_a$  of the image was correlated with the  $R_a$ . A normalized power spectrum was obtained from the experimental images. The effect of cutting speed, feed, and depth of cut and fiber orientation angle on surface roughness was studied. However, this method is prone to errors caused by the blurring effect due to the low resolution (768×574 pixel) images captured using a CCD camera.

Shahabi and Ratnam (2009b) published a novel method for measuring the roughness of turned parts using machine vision. A CCD camera was mounted on the lathe and used to capture images of the workpiece profile with the aid of back lighting. The silhouette of the surface profile was processed using algorithms developed in MATLAB to extract the surface roughness parameter  $R_a$ . The roughness measurement using vision method was compared with the conventional stylus method and an agreement within 10% was observed. However, the lathe machine was stopped before an image of the work piece was captured, thus rendering the technique, at most intermittent.

### **2.2.2 Surface roughness measurement in other machining processes using machine vision approach**

Applications of the machine vision approach for measuring the surface roughness in milling, grinding and lapping process have been reported in some studies. Surface roughness monitoring using computer vision was investigated by Sodhi and Tiliouine (1996) in the surface grinding process. Surface roughness measurement using the speckle pattern caused by a laser beam on a rough surface was introduced. The method was applied for tracking the roughness of a workpiece being processed on a surface grinder. The author concluded that an investigation with a broader range of wavelengths of the light is required to validate the measurement.

Wang et al. (1998) developed a machine vision technique, termed as dark bright ratio method, which utilizes the size of dark or bright area in the image to interpret the roughness of a lapped and ground specimen. A speckle pattern was formed by projecting the laser beam onto the specimen surface in stationary and rotational conditions. However, the accuracy and consistency of their technique in obtaining roughness data of surfaces was proven only up to the linear speed of 0.107 m/s (60 rpm).

Younis (1998) introduced an online surface roughness measurement method using machine vision. A white light scattered from the stationary grinded specimen was captured using a CCD camera. The image-based '*grey level coefficient*' parameter that gives the correlation between the grey levels at any point in the image to the surrounding point was investigated. The relationship between the measured optical roughness parameter for

different type of materials and the  $R_a$  were studied for repeatability analysis. The coefficient of variation of the  $R_a$  measured using the machine vision method was reported as 8.6% compared to 15% for the stylus method. However, the measurement was carried out on a stationary grinded specimen.

In another research, Wong and Li (1999) developed an in-process surface roughness measurement technique for moving surface in a cylindrical grinding process using the combined effect of interference and light scattering principle. The speckle patterns formed by the reflections of a laser beam were used for the roughness measurement. The bright and dark intensity ratio in the image was correlated to the  $R_a$ . The surface roughness of six standard flat grinded surfaces was measured and the roughness values were verified with the stylus instruments. The roughness was measured in-cycle and the grinding wheel was at the end position of its stroke. Thus, the proposed method is not an in-process measurement technique.

An in-process optical method for measuring the surface quality using modified Beckmann–Kirchhoff (B-K) scattering theory was proposed by Guo and Tao (2009). The mean scattered intensity distributions from a grinded specimen surface with and without the fluid layers were analyzed. The experiment was conducted with pixel grey value measurement along the main direction of light scattering stripe to validate the modified B–K scattering theory. However, the experiments were conducted on standard pre-lapped and grinded flat steel specimens.

Dhanasekar and Ramamoorthy (2010) captured the images of moving milled surfaces using machine vision method and then de-blurred the images using Richardson–Lucy restoration algorithm. The de-blurred images were pre-processed

to compensate the inhomogeneous illumination. The surface texture features such as spatial frequency, arithmetic mean value and standard deviations were extracted and used as input to the Artificial Neural Network (ANN) model to predict the surface roughness. The results from vision system and stylus method were compared to show a good correlation. However, this method can only be used for milled and grinded surfaces moving at speed of 25.4 mm/s.

Guo and Tao (2010) investigated the optical characteristics of a laser beam passing through a static and a flowing fluid layer on a standard grinded specimen for in-process surface roughness measurement. Laser beam propagation through a static and dynamic transparent fluid layer and its effects were analyzed using modified B-K scattering theory. The parameter  $R_a$  was estimated from a selected ratio parameter of the light-scattered images of the specimens. Experiments were also conducted for different fluid flow rates. It was concluded that the propagation of the laser beam in the transparent region was not affected by the flowing properties of the fluid layer. The surface roughness parameters were in close agreement with the modified B-K scattering theory. However, the experiments were conducted only on grinded flat steel specimens with known surface roughness values. Furthermore, only the  $R_a$  was used for the analysis.

Guo and Tao (2011) proposed a modified B-K scattering theory for in-process roughness measurement of a grinded flat surface with transparent additional layers. The  $R_a$  was extracted based on the light scattering principle and machine vision method to verify the correction of the modified B-K scattering theory. Test specimens with different surface roughness were studied using a collimated laser diode, beam splitter and a camera. Roughness values were calculated from the fitting formula from the light scattered image. The relationship

between the ratio parameter extracted from the light scattering image and surface roughness was obtained by curve fitting. Test specimens with different surface roughness were chosen to verify the surface with and without additional layers in the modified B-K scattering model. The model was verified by measuring the roughness values of a surface with and without the additional layers. The change of the mean scattered intensity distributions from a surface was described by a newly introduced attenuation factor. It was concluded that the modified B-K scattering model with attenuation factor can be used as the theoretical basis for in-process optical measurement of surface characteristics. However, it is necessary to conduct a series of experiments to testify the validity of this model.

Guo and Tao (2013) presented a method with light scattering principle and machine vision technique to estimate the surface roughness of lapped specimens. Laser beams were allowed to pass through transparent layers and reach the workpiece surface for measuring the surface roughness. The inaccessibility problem caused by the opaque property of the coolants was overcome by providing an optically clean zone using a transparent window. The surface scattered images of the specimens were acquired by machine vision system and the roughness parameters were extracted from the images. Features of the surface texture image were extracted and scattering data were analyzed by using light scattering technique and neural network model. However, the surface roughness was not measured during the machining process.

Many researchers have attempted to measure the surface roughness using machine vision. However, no published studies have explored an in-process method for measuring the surface roughness in other machining process using machine vision approach.

### 2.2.3 Sensor approach for in-process surface roughness assessment

In-process surface roughness assessment model based on regression, ANN, fuzzy logic and neuro-fuzzy have been attempted by many researchers. Signals such as cutting forces, vibrations and workpiece surface temperature that represent the interaction between the tool and workpiece during the machining process were used as inputs for the in-process surface roughness estimation model. Dynamometers, accelerometers and infrared thermometers are the most commonly used sensors in the in-process surface roughness estimation model.

In-process surface roughness estimation using cutting force sensing is proposed in few researches. Suksawat (2011) developed an in-process surface roughness estimation method in turning operation using data acquisition system and fuzzy logic system. A miniature load cell and signal interface cards were used to detect the cutting force signal. The detected cutting force signal was transmitted to a data analysis module. Twenty fuzzy rules were developed based on the correlation between the cutting speed, feed rate and cutting force and were used to estimate the  $R_a$ . It was concluded that the estimated surface roughness values were close to the conventional stylus surface roughness measurement. However, only the  $R_a$  was estimated during turning of polymeric materials.

Somkiat and Voraman (2012) proposed an in-process system that predict and control the surface roughness during the turning process. A tool dynamometer was used to measure the feed force and the cutting force. The force ratio was used to estimate the surface roughness. The upper control limit and the lower control limits of surface roughness values were calculated using the *Individual and Moving Range* (I-MR) chart to monitor and control the process capability during the turning

process. The calculated upper and the lower control limits of surface roughness values were used in the I-MR charts for the in-process statistical process control for the mass production run. The control limits were used as warning system for the out-of-control surface roughness. However, only  $R_a$  and Ten point average height roughness parameter ( $R_z$ ) were used for the surface quality assessment.

Some researchers have reported the in-process surface roughness estimation using vibration signals. Lou and Chan (1999) obtained in-process surface roughness information by processing the vibration data collected with an accelerometer. The analysis of the data and the developed model was carried out using a neural fuzzy system. The spindle speeds, feed rate, depth of cut and vibration variables were used to predict the surface roughness effectively. However, the model was used to estimate the  $R_a$  in the end milling process.

Kirby et al. (2006) developed a fuzzy-net based in-process surface roughness adaptive control system during the finish turning process using vibration. A series of validation runs were conducted to find out the surface roughness specifications and to adjust the machine tool to obtain the desired surface roughness. The authors commented that the model accuracy can be improved by considering the other process variables such as noise factor, different cutting tools and workpiece materials. However, the system requires fine tuning of the model to predict the surface roughness and to adapt the machining parameters to achieve the surface roughness within the specified tolerance.

Julie et al. (2007) proposed an in-process surface roughness adaptive control system during the turning process using cutting tool vibration. An accelerometer sensor and an ANN were integrated to predict and control the surface roughness.



The detected vibration signals were used to predict the surface roughness and to adapt the cutting parameters. However, the predicted  $R_a$  values were lower than the desired values.

In another research using vibration signals, an in-process surface roughness prediction system based on least-squares support vector machines for turning process was reported by Salgado et al. (2009). A singular spectrum analysis was used for processing the cutting vibration signals and to correlate with surface roughness. The machining conditions such as feed rate, cutting speed, and depth of cut with the features extracted from the vibration signals were mainly constituted as input information to the system. It was recommended that the accuracy of a surface roughness prediction system based on cutting vibrations could only be improved by including input information about tool geometry, as well as cutting conditions. In addition, a tri-axial accelerometer was recommended for the development of an accelerometer-based surface roughness prediction system.

A multi-sensory approach for the in-process surface roughness prediction in turning process using vibration and cutting force was proposed by Upadhyay et al. (2013). First order and second order multiple regression models were developed to predict the  $R_a$  using acceleration amplitude of tool vibrations in the axial, radial and tangential directions. The correlation between the surface roughness and the cutting parameters and acceleration amplitude of vibrations was found by using Pearson correlation coefficient. It was concluded that the Pearson correlation model was more accurate than the first and second order multiple regression models.

Sensing the surface temperature of the workpiece during machining is another method proposed for the in-process estimation of the surface roughness. Suhail et al. (2011) proposed an in-process regression model to predict the  $R_a$  based on the workpiece surface temperature acquired by an infrared thermometer during the turning process. The surface temperature of the workpiece was correlated to the surface roughness and the relationship between the workpiece surface temperature and the cutting parameters were also found. Regression equations were established using the statistical analysis software to obtain the relationship between the different response variables such as surface roughness and workpiece surface temperature and the input parameters such as speed, feed, and depth of cut. Thirty three full factorial design was used to get the output data uniformly distributed over the ranges of the input parameters. The surface was cleaned after each machining pass and the  $R_a$  was measured with the contact profilometer. As the feed rate increased the surface roughness increased and workpiece surface temperature decreased. The higher workpiece surface temperature resulted in better surface roughness.

The majority of the in-process surface roughness estimation using sensor approach uses the neural network model. However, the extensive training of the neural networks is a major drawback. In addition, these methods were developed only for the prediction of the basic amplitude surface roughness parameters, such as  $R_a$  and  $R_q$ . Since tool wear is a significant factor affecting the machined surface finish quality, the classification of wear and the various types of tool wear monitoring in turning process and their effectiveness in surface quality assessment in finish turning process is discussed in the following section.

### 2.3 TWM in turning

Tool wear is the major problem in a turning process and has been studied extensively in the past in order to prevent inferior surface finish quality. According to International standard ISO 3685 (1993), four types of cutting tool wear are observed in turning process. These are (i) crater wear (ii) wear of the major flank (iii) wear of the rake face and (iv) wear of the minor flank. The various types of cutting tool wear are illustrated in Figure 2.1.

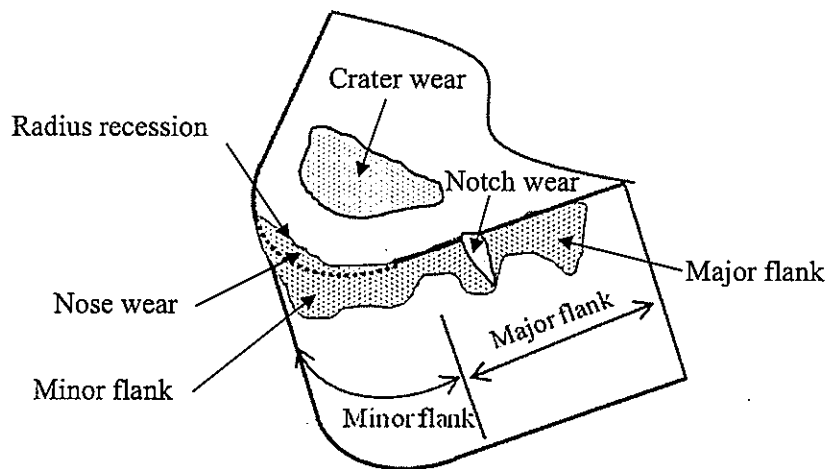


Figure 2.1. Typical cutting tool wear.

Crater wear occurs at the rake face as a result of high thermal and shear stress due to the chip thickness as shown in Figure 2.2(a). The major flank wear is shown in Figure 2.2(b) and is the best known criterion of tool wear. The common criteria used for the assessment of flank wear is  $VB_{max} = 0.6$  mm if the flank wear is not regularly worn, scratched, chipped or badly grooved in zone B. The average width of the flank wear land  $VB = 0.3$  mm if the flank wear land is considered to be regularly worn in zone B. The combined wear of flank and

the rake face wear forms the notch wear (Figure 2.2(b)) at the depth of cut line when the tool rubs against the shoulder of the workpiece.

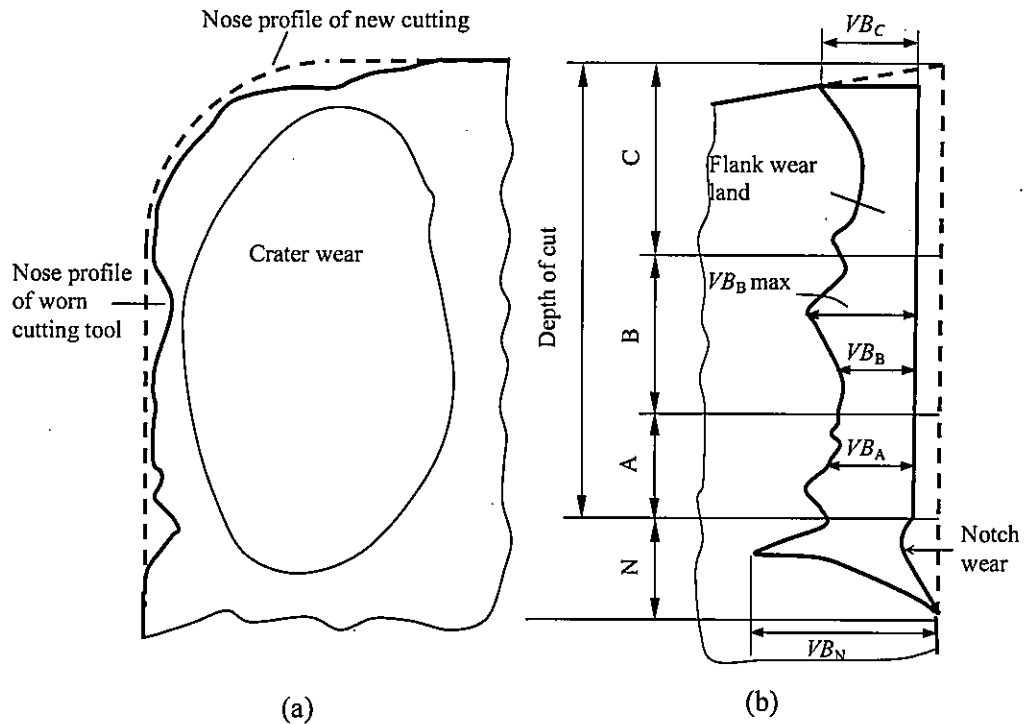


Figure 2.2. (a) Top view of crater wear and nose profile (b) flank wear land and notch wear of cutting tool based on ISO 3685 (1993).

The existing TWM methods are focused only on the monitoring of the flank wear (Wang et al. 2011; Rajesh and Narayanan, 2010; Wang et al. 2006; Kerr et al. 2006; Jurkovic et al. 2005) and crater wear (Wang et al. 2011; Devillez et al. 2004). However, the nose radius wear that occurs on nose region of the cutting tool is the most noticeable and significant wear in the finish turning process (Bhuiyan et al. 2014). The nose radius wear occur mainly due to the abrasion wear mechanism of cutting tool's major edges resulting in an increase in negative rake angle where the nose edge deform plastically. The nose radius wear is the major wear criterion in finish turning process since the cutting action is mainly

undertaken by the tool nose. Since the depth of cut and feed is less than the nose radius of the cutting insert in finish turning process, the nose region of the cutting tool is considered to be worn. Only after the tool nose region is worn away, the tool flank and crater wear begin to dominate.

The nose radius wear flattens the tool nose thus affecting the surface quality of the finished work piece, machining stability, heat generation, residual stress as well as the condition of the insert due to the direct interaction of the tool nose with the workpiece during the finish turning. In addition, the nose radius wear gradually increases the dimension of the machined surface, thus introducing significant dimensional errors which could reach 0.03 to 0.05 mm (Prasad et al. 2011). The micro geometric variations in the workpiece surface profile caused by the progressive tool nose radius wear, however, have not been explored in the past. The deformation process during the machining is normally accompanied by the rubbing action with high friction that generates heat in plastic deformation. In finish turning, the nose area, which is located at the tool-chip interface and tool-work contact surface, is subjected to the most severe rubbing action. Thus, the nose area wears down due to its lower strength and wear resistance when the temperature increases. According to ISO 3685 (1993), nose deformation will in most cases lead to a more rapid occurrence of catastrophic failure of high-speed steel tools and this makes the consequences of oxidation of carbide tools more severe.

Different approaches and different measures have been used to determine the amount of wear, both qualitatively and quantitatively. The various techniques proposed for monitoring the tool wear are generally classified into direct and indirect method (Gao et al. 2015). In the direct method, the actual value of certain

wear parameter on the tool is measured directly by way of the tool images. Although the application of the direct tool wear assessment systems by means of the tool images is simple and highly reliable, the in-process application of a direct tool wear estimation system is difficult since the turning process must be interrupted to make the measurements. Indirect methods utilize a suitable process-borne signal from the sensors to assess the degree of tool wear. Methods of tool wear monitoring as well as the machine vision approach used for tool wear monitoring are reviewed in the following section.

### **2.3.1 Direct TWM using machine vision**

Machine vision systems have been used to assess the tool condition either directly or indirectly. Direct methods are based on the measurement of worn area of the cutting tool (Lanzetta, 2001). Indirect methods utilize the image of the machined workpiece surface to monitor the tool condition without cutting tool observation.

Direct tool condition monitoring using machine vision approach uses a high resolution CCD camera to capture the image of the used cutting tool between cutting cycles or cutting tool passes. Various image processing techniques and visualization methods have been published to characterize the tool wear. Kurada and Bradly (1997) presented a vision method with a series of simple image analysis algorithms to derive morphological parameters, which are the maximum nose flank wear, area and perimeter of wear region. A CCD camera and two fiber optic illuminators were used to capture images orthogonal to the flank face. The relationship between the cutting time and the wear-land width was investigated. The author suggested that the compactness is a sensitive parameter to indicate the

approximate starting point for the notch wear and the variance operator was best suited for detecting the wear. The authors commented that the actual wear region identification and measurement relies on the specular reflection of the wear area from the fiber optic lights. Even though the results were promising as the wear measurements were repeatable and comparable with toolmaker's microscopes, however, the vision system was not integrated to a turning machine.

Pfeifer and Wieger (2000) used optimized tool wear image from different tool wear images obtained from different illumination for tool wear assessment. Comparison was made among the different illuminated images and the contour degree of overlap (DOV) was computed to identify the real edges of tool wear. However, the assessment takes longer time since more than one image must be captured for comparison purposes to get the 'real wear edges'.

A high-resolution vision sensor with changeable lighting conditions for tool flank and crater wear assessment was proposed by Lanzetta (2001). The tool wear images were captured using different resolutions ranging from low to high. Grey-scale images were taken from the nose of the tool and images of the tool silhouette were taken from the top of the tool. Silhouette is taken with a back light and the tool nose is directly illuminated. Images were also taken with directional light from the top of the tool to detect crater wear. The images captured were then combined by morphological union using an averaging method. Flank wear was measured from the silhouette image. The silhouette of the worn tool was compared to the silhouette of the unused tool. However, this method requires a minimum of four tool wear images in order to obtain the final image for the segmentation. Prasad et al. (2011) measured the crater wear using stereo-vision.